International Journal of Nanomedicine

Dovepress
open access to scientific and medical research

Open Access Full Text Article

ORIGINAL RESEARCH

Cascade-Targeting of Charge-Reversal and Disulfide Bonds Shielding for Efficient DOX Delivery of Multistage Sensitive MSNs-COS-SS-CMC

This article was published in the following Dove Press journal:
International Journal of Nanomedicine

Lan Cui[1,*]
Wentao Liu[1,*]
Hao Liu[1]
Qian Qin[1,2]
Shuangxia Wu[1]
Suqin He[1,3]
Zhenya Zhang[4]
Xinchang Pang[1]
Chengshen Zhu[1]

[1]School of Materials Science and Engineering, Zhengzhou University, Zhengzhou 450001, People's Republic of China; [2]Bio & Soft Matter, Institute of Condensed Matter and Nanosciences, Universite Catholique de Louvain, Louvain-la-Neuve B-1348, Belgium; [3]Henan Key Laboratory of Advanced Nylon Materials and Application, Zhengzhou University, Zhengzhou 450001, People's Republic of China; [4]Department of Chemistry, Changwon National University of Korea, Changwon-city, Gyeongnam-do 51140, Republic of Korea

*These authors contributed equally to this work

Correspondence: Wentao Liu; Hao Liu
School of Materials Science and Engineering, Zhengzhou University, Zhengzhou 450001, Henan Province, People's Republic of China
Email wtliu@zzu.edu.cn; hliu@zzu.edu.cn

Background: Although pH and redox sensitiveness have been extensively investigated to improve therapeutic efficiency, the effect of disulfide bonds location and pH-triggered charge-reversal on cascade-targeting still need to be further evaluated in cancer treatment with multi-responsive nanoparticles.

Purpose: The aim of this study was to design multi-responsive DOX@MSNs-COS-NN-CMC, DOX@MSNs-COS-SS-CMC and DOX@MSNs-COS-CMC-SS and systematically investigate the effects of disulfide bonds location and charge-reversal on the cancer cell specificity, endocytosis mechanisms and antitumor efficiency.

Results: In vitro drug release rate of DOX@MSNs-COS-SS-CMC in tumor environments was 7-fold higher than that under normal physiological conditions after 200 h. Furthermore, the fluorescence intensity of DOX@MSNs-COS-SS-CMC and DOX@MSNs-COS-CMC-SS was 1.9-fold and 1.3-fold higher than free DOX at pH 6.5 and 10 mM GSH. In addition, vesicular transport might be a factor that affects the uptake efficiency of DOX@MSNs-COS-SS-CMC and DOX@MSNs-COS-CMC-SS. The clathrin-mediated endocytosis and endosomal escape of DOX@MSNs-COS-SS-CMC enhanced cellular internalization and preserved highly controllable drug release into the perinuclear of HeLa cells. DOX@MSNs-COS-SS-CMC exhibited a synergistic chemotherapy in preeminent tumor inhibition and less side effects of cardiotoxicity.

Conclusion: The cascade-targeting of charge-reversal and disulfide bonds shielding would be a highly personalized strategy for cervical cancer treatment.

Keywords: disulfide bonds, pH-triggered charge-reversal, redox sensitive, chitosan oligosaccharide, human cervical carcinoma therapy

Introduction

Tumor microenvironment stimuli-sensitive nanoparticles are of considerable implication in improving non-specific drug internalization and tumor-targeted therapy. Among the internal/external stimuli (pH,[1,2] redox,[3,4] enzymes,[5,6] temperature,[7–9] magnetic forces[10,11] and ultrasound,[12,13] etc.), redox-stimulus has been utilized to prompt the rapid and sufficient drug release in the intracellular microenvironment, wherein disulfide linkage would be rapidly broken up in the reductive environment (glutathione, 2–10 mM).[14,15] Studies have shown that the exposed disulfide bonds may be destroyed by protein disulfide isomerase on the surface of cell membrane during endocytosis,

which inevitably affect drug release efficiency through the location of disulfide bonds.[16,17] The current challenge is to prompt efficient endosomal escape and improve the degradation of nanoparticles in the cytoplasm of cancer cells.[18,19]

On the other hand, in view of the pH variation in tumor tissues (pH 6.5–6.9), endo/lysosomes (pH 5.0–5.5) and normal physiological environment (pH 7.4),[20–22] pH-induced charge-reversible nanoparticles have been extensively reported to spontaneously improve cellular uptake and controllable drug release through the enhanced permeability and retention effects.[23,24] The negative charge renders nanoparticles with stealth characteristics to avoid non-specific protein binding and prolong retention time.[25,26] The positive charge of nanoparticles could induce cell membranes rupture and facilitate endosomal escape due to the proton sponge mechanism.[27,28] Charge-reversible chitosan shell has been designed as a switchable pore-capping agent and membrane-destabilization moiety in our previous research.[29] Nevertheless, how to improve the charge-reversal response, facilitate the biodegradability and prompt the efficient drug delivery into nucleus remains an urgent problem to be solved in the drug delivery system.[30,31] Thus, it is highly desirable to design multifunctional nanoparticles that simultaneously respond to complicated microenvironments.[32]

Herein, pH-triggered charge-reversible and redox multi-responsive nanoparticles were designed for on-demand delivery of doxorubicin hydrochloride (DOX) through self-assembly of disulfide-containing chitosan oligosaccharide and carboxymethyl chitosan (COS-SS-CMC and COS-CMC-SS) and mesoporous silica nanoparticles (MSNs). The purpose of this study is to design multistage-responsive nanoparticles and evaluate the effect of cascade-targeting of surface charge reversal and disulfide bonds location on the endocytosis mechanism and antitumor efficiency.

As shown in Figure 1, negative-charged shield and charge reversal were sequentially realized to facilitate intracellular uptake and endosomal escape via the protonation/deprotonation effect and proton sponge effect after cellular endocytosis. Disintegrations of DOX@MSNs-COS-SS-CMC promote burst release, efficient drug delivery into the nucleus and instantaneous apoptosis of HeLa cells at the presence of over-expressed glutathione (GSH). Thus, the multistage drug-delivery system would improve the tumor-targeted uptake through pinpointed cascade of pH-triggered charge-reversal and disulfide bonds breakage, which would provide a viable strategy for the treatment of human cervical carcinoma.

Experimental Section

Materials

Tetraethyl orthosilicate, chitosan (M_w, 200 kDa; deacetylation degree, 85%), sodium tripolyphosphate, doxorubicin hydrochloride (DOX) and dimethyl sulfoxide were obtained from Aladdin Chemistry Co., Ltd. (Shanghai, China). Chitosan oligosaccharide (COS, M_w, 3 kDa; deacetylation degree, 80%) was purchased from Golden-Shell Biochemical Co., Ltd. Diallyl disulfide, N,N′-methylenebisacrylamide, nitric acid and acetic acid were purchased from Macklin Biochemical Co., Ltd. Ceric ammonium nitrate, acrylic acid and methyl methacrylate were purchased from Sinopharm Chemical Reagent Co., Ltd. Glutathione was purchased from Beijing Dingguo Changsheng Biotechnology Co., Ltd.

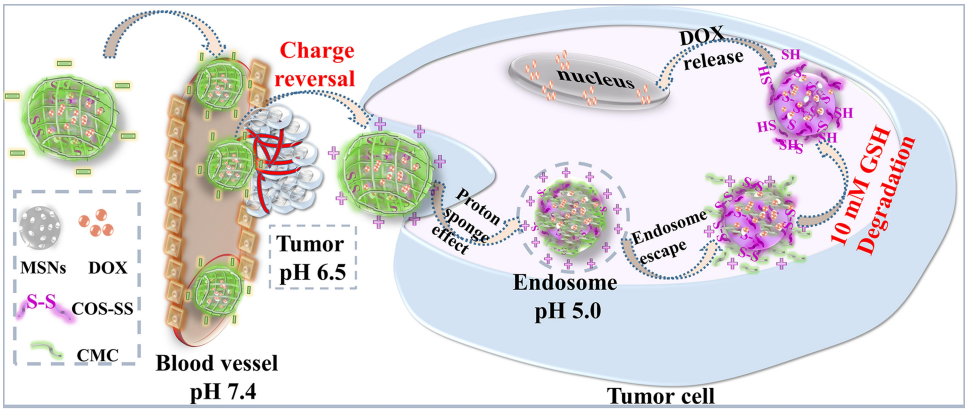

Figure 1 Schematic illustration of DOX release of charge-reversible and pH-redox dual sensitive DOX@MSNs-COS-SS-CMC.
Abbreviations: MSNs, mesoporous silica nanoparticles; DOX, doxorubicin hydrochloride; COS-SS, disulfide-containing chitosan oligosaccharide; CMC, carboxymethyl chitosan; GSH, glutathione.

Human cervical carcinoma cells (HeLa cells) and female BALB/c nude mice (5–6 weeks old, 18 ± 2 g) were supplied by Institute of Virology, Chinese Academy of Sciences. HeLa cells were cultivated in Dulbecco's Modified Eagle medium containing 10% fetal bovine serum and 1% antibiotics. All cell line and animal experiments were executed in compliance with the Animal Management Rules of the Ministry of Health of the People's Republic of China and approved by the Animal Care and Ethics Committee and Institutional Review Board of Wuhan Institute of Virology, Chine Academy of Sciences (Approval No. WIVA20201802).

Preparation of COS-SS, CMC-SS and COS-NN

The disulfide-containing chitosan oligosaccharide (termed as COS-SS) was fabricated according to the method described by Wang et al[33] with a slight modification. COS (1.0 g; M_w, 3 kDa) was dissolved in acetic acid (2%, V/V) under N_2 protection and magnetically stirred at 30°C for 0.5 h. Ceric ammonium nitrate (0.5 g dissolved in 2.5 mL of 0.1 mol/L nitric acid) was added as initiator and stirred for 5 min. Subsequently, acrylic acid (0.4 mL) was added dropwise to the solution at 60 ºC for 1 h, and methyl methacrylate (0.6 mL) was mixed with the mixture for 0.5 h. Then, diallyl disulfide (0.7 mL dissolved in 1 mL of dimethyl sulfoxide) was added as crosslinking agent and stirred for 12 h, the molecular ratio of COS, acrylic acid, methyl methacrylate, ceric ammonium nitrate and diallyl disulfide was 7:7:7:1:0.7. The sample was purified by dialysis and obtained after freeze-drying at a yield of 80% (Yield%=$W_{product}/(W_{COS} + W_{monomer} + W_{crosslinker}) \times 100\%$, W means product weight).

Carboxymethyl chitosan (CMC, substitution degree, 92%; Y_{-NH2}, 56%) was synthesized by the method described by Chen et al.[34] The disulfide-containing carboxymethyl chitosan (termed as CMC-SS) was designed through the same process of COS-SS. COS was replaced by the addition of CMC (1.2 g; M_w, 200 kDa). Subsequently, Ceric ammonium nitrate (0.5 g), acrylic acid (0.4 mL), methyl methacrylate (0.6 mL) and diallyl disulfide (0.7 mL) were added into the system, respectively. The sample was obtained after freeze-drying at a yield of 85%.

In addition, the non-cleavable chitosan (COS-NN) was designed as a control through the same process. N,N′-methylenebisacrylamide (0.1 g) was chosen as the crosslinker to replace the disulfide bond-containing diallyl disulfide.

Construction of DOX-Loaded Nanoparticles

MSNs were designed according to our previous research.[32] DOX@MSNs-COS-SS-CMC were designed by ionic crosslinking self-assembly method.[32] MSNs (10 mg) were dispersed in phosphate buffer solution (10 mL, pH 7.4) and stirred in dark after the addition of DOX (1 mg/mL, 5 mL) for 24 h. The reaction was conducted at 60°C for 0.5 h after the dropwise injection of sodium tripolyphosphate (0.25 mg/mL). Subsequently, COS-SS (2.5 mg/mL, 20 mL) was mixed with the suspension and stirred at 30°C for 2 h, followed by the interaction of CMC (1 mg/mL) for another 2 h. DOX@MSNs-COS-SS-CMC were obtained after centrifugation and freeze-drying.

In addition, DOX@MSNs-COS-NN-CMC and DOX@MSNs-COS-CMC-SS were prepared through the same process of DOX@MSNs-COS-SS-CMC. COS-NN (2.5 mg/mL, 20 mL) and CMC-SS (2 mg/mL, 20 mL) were chosen to replace the COS-SS and CMC, respectively.

In vitro Drug Release

DOX-loaded nanoparticles were dispersed in dialysis membranes containing phosphate buffer solution and different concentrations of glutathione at 37°C and 100 rpm, simulating the drug release in the intracellular and extracellular environment. Release media were withdrawn and replenished with corresponding fresh media at the appropriate intervals. The cumulative drug release at different pH variations and glutathione concentrations was calculated by ultraviolet spectrophotometer.

Characterization

The chemical structures of samples were measured by X-ray photoelectron spectra (XPS, Axis Supra, Kratos), proton nuclear magnetic resonance (^{1}H NMR, AVIII HD 600 spectrometer, Bruker) and Fourier transform infrared spectroscopy (FT-IR, VERTEX70 spectrometer, Bruker). DOX concentration was calculated by ultraviolet spectrophotometer using UV-721G (Jingke). The morphologies of samples were visualized by transmission electron microscopy using Hitachi-HT7700. The zeta potential and particle size distribution were analyzed by dynamic light scattering using Malvern Zetasizer Nano ZS90.

In vitro Cytotoxicity

The cytotoxicity of free DOX, DOX@MSNs-COS-NN-CMC, DOX@MSNs-COS-SS-CMC and DOX@MSNs-COS-CMC

-SS against HeLa cells was analyzed by CCK-8 assay. HeLa cells (1×10^4 cells/well) were seeded in 96-well plates and incubated for 24 h. The culture media were replaced with fresh media containing DOX-loaded nanoparticles at equivalent DOX concentration. After 24 h of incubation, fresh media containing CCK-8 solution were appended in each well after the rinse of phosphate buffer solution. The cytotoxicity was calculated by multimode plate reader (EnSpire, PerkinElmer, USA) at 450 nm after 3 h of incubation.

Intracellular Uptake and Subcellular Localization Assays

The cellular internalization and bio-distribution were evaluated by confocal laser scanning microscope (CLSM) using Nikon eclipse Ti confocal microscope. HeLa cells (1×10^5 cells/dish) were seeded in glass-bottomed dishes for 24 h. Afterwards, the culture media were replaced with fresh media including free DOX, DOX@MSNs-COS-NN-CMC, DOX@MSNs-COS-SS-CMC and DOX@MSNs-COS-CMC-SS (DOX, 2 μg/mL). After incubation for 24 h, cells were fixed with paraformaldehyde at 4 ºC for 15 min and cell nuclei were stained with Hoechst 33342 for 5 min.

The subcellular localization was also analyzed by CLSM to evaluate the endosomal escape of DOX-loaded nanoparticles (DOX, 2 μg/mL) in HeLa cells (1×10^5 cells/dish) at pH 6.5 and 10 mM GSH. After the incubation of Hela cells with DOX-loaded nanoparticles for 1, 3 and 8 h, the endo/lysosomes were stained with LysoTracker Green for 30 min, and nucleus were stained with Hoechst for 5 min, respectively. The fluorescence signals in endo/lysosomes and nucleus were analyzed by Image J software.

Quantitative Evaluation of Cellular Internalization and Endocytic Pathway

The fluorescence intensity was analyzed by flow cytometer (BD LSRFortessa, USA). HeLa cells (2×10^5 cells/well) were cultured in 6-well plates. After the treatment with DOX-loaded nanoparticles (DOX, 2 μg/mL), cells were collected and digested by trypsin for 2 min. Subsequently, HeLa cells were dispersed into phosphate buffer solution (0.25 mL) to determine the fluorescence intensity after centrifugation.

The endocytic pathway was also evaluated by flow cytometry analysis. HeLa cells (2×10^5 cells/well) were pretreated with endocytic inhibitors (4 μg/mL of chlorpromazine, 100 μg/mL of amiloride, 0.5 μg/mL of nocodazole and 60 μg/mL of genistein) for 1 h, which were used to interfere with the clathrin-mediated endocytosis, macropinocytosis, vesicular transport and caveolin-mediated endocytosis, respectively.[35] Then, HeLa cells were incubated with DOX-loaded nanoparticles (DOX, 2 μg/mL) at pH 6.5 and 10 mM GSH. After incubation for 5 h, HeLa cells were collected to determine the fluorescence intensity by flow cytometry.

In vivo Therapeutic Efficiency and Histological Study

The female BALB/c nude mice (5–6 weeks old, 18±2 g) were fed under specific pathogen-free environments and acclimatized for one week prior to experiments. HeLa cells (10^6 cells) were injected into female BALB/c nude mice to establish a subcutaneous xenograft tumor model. When the tumor volume approximately reached 100 mm^3, tumor-bearing mice were randomly assigned into five groups and injected intravenously with saline solution, free DOX, DOX@MSNs-COS-NN-CMC, DOX@MSNs-COS-SS-CMC and DOX@MSNs-COS-CMC-SS (DOX, 5 mg/kg) every 2 days. The injections were repeated seven times over a 15-day treatment period. Tumor volume was quantified by the formula: $V=Width^2\times Length/2$. DOX bio-distribution in the tumor and normal tissues was analyzed using the IVIS system and the Maestro CRi software after 3, 7 12 and 24 h post-injection. All the mice were sacrificed after 15 days, the tumors and major organs (heart, liver and kidney) were collected and embedded in paraffin for histological examinations. Tissue slices were stained with hematoxylin and eosin (H&E). The systemic toxicity of DOX-loaded nanoparticles in mice was analyzed by optical microscope (Chirascan-SF, Thermo & 3DHISTECH, USA).

Statistical Analysis

Statistical results are expressed as mean ± standard deviation and the statistical significance of the differences was analyzed by SPSS 21.0 software using one-way analysis of variance (ANOVA) and Student's *t*-test. *Means $P < 0.05$, **Means $P < 0.01$ and ***Means $P < 0.001$, respectively.

Results and Discussion

Redox and Charge-Reversal Characterization of DOX@MSNs-COS-SS-CMC

As illustrated in the XPS analysis (Figure 2A and B), C 1s peak derived from C-C, C-N, C-S, C=O and -COO- bonds, S 2p peak was divided into three components at 163.3, 164.6 and 168.1 eV.[36] In addition, ^{1}H NMR and FT-IR spectra analysis (Figures S1–3) certified the triumphant incorporation

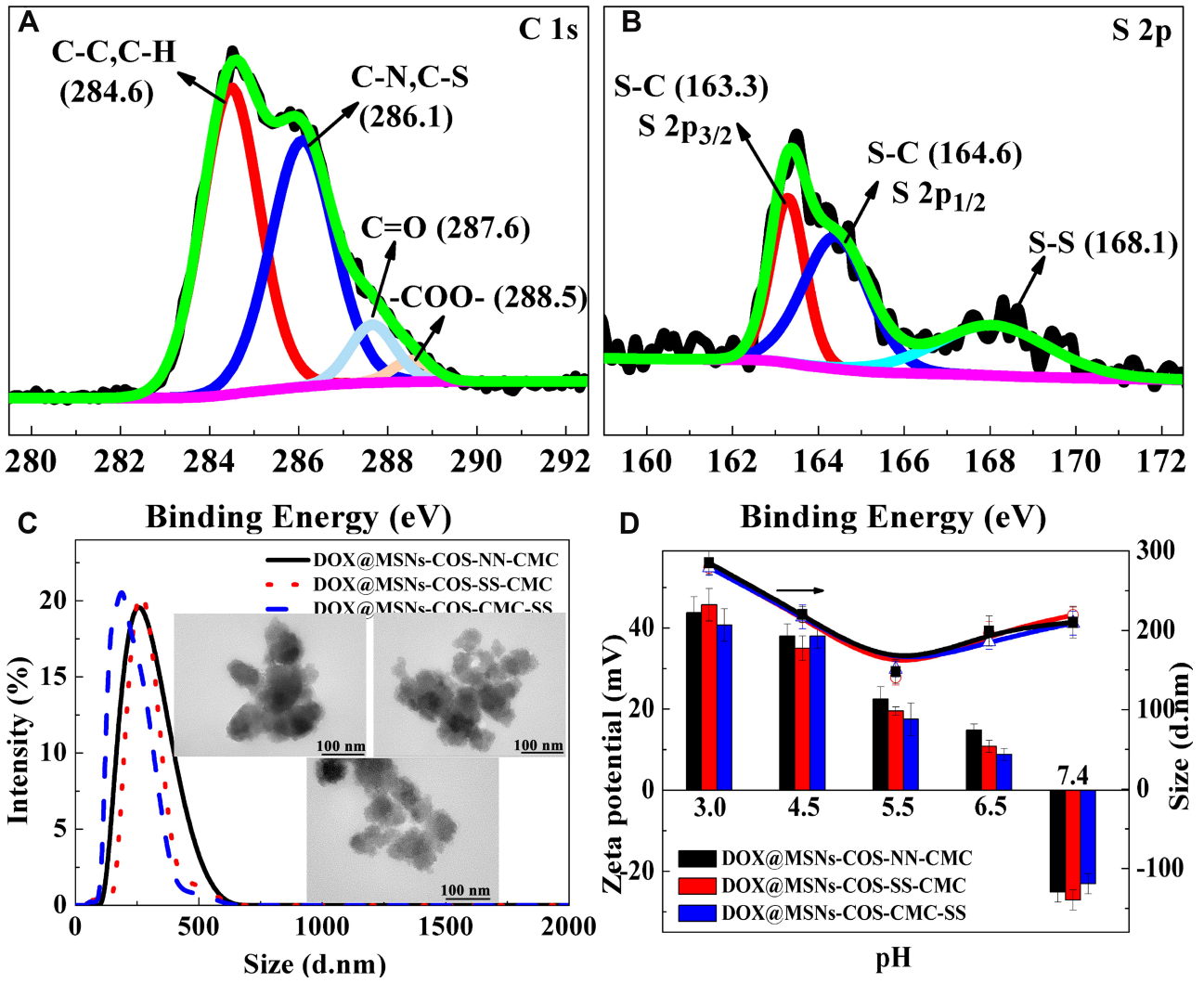

Figure 2 Redox characterizations and charge-reversal of DOX@MSNs-COS-NN-CMC, DOX@MSNs-COS-SS-CMC and DOX@MSNs-COS-CMC-SS. (**A** and **B**) C 1s and S 2p XPS spectra of DOX@MSNs-COS-SS-CMC. (**C**) Particle size distribution (Inside, TEM images). (**D**) Charge-reversal by pH trigger.

Abbreviations: MSNs, mesoporous silica nanoparticles; DOX, doxorubicin hydrochloride; COS, chitosan oligosaccharide; COS-SS, disulfide-containing chitosan oligosaccharide; COS-NN, non-cleavable chitosan, diallyl disulfide was replaced by N,N′-methylenebisacrylamide; CMC, carboxymethyl chitosan; CMC-SS, disulfide-containing carboxymethyl chitosan.

of DOX and COS-SS-CMC shell, the encapsulation efficiencies of DOX-loaded nanoparticles were significantly increased to 93±4% (Table S1). As shown in Figure S1, the peak at 1.70 ppm was attributed to the methyl of acetyl groups, peaks between 1 and 2.5 ppm were ascribed to the chemical shifts of -CH_2 and -C-H of acrylic acid, methyl methacrylate and diallyl disulfide. Characteristic peaks at 3.15 and 4.26 ppm revealed the carboxymethyl substitution of CMC-SS at C_2-NH_2 and C_3-OH and C_6-OH. Moreover, as illustrated in Figures S2 and S3, the adsorption peak at 1237 cm^{-1} corresponded to the stretching vibration peak of -S-S-. The adsorption peaks at 1080 and 800 cm^{-1} were the asymmetric and symmetric vibration peaks of Si-O-Si. DOX@MSNs-COS-SS-CMC exhibited the absorption peaks at around 1735, 1647 and 1557 cm^{-1}, owing to the stretching vibration of -COO-, N-H and C-N, respectively. The adsorption peaks at 2927 and 2849 cm^{-1} were the asymmetric and symmetric vibration peaks of -C-H. The above results reveal the encapsulation of DOX and disulfide bond.

The particle size and morphology of nanoparticles were measured by dynamic light scattering and transmission electron microscopy (TEM) as shown in Figure 2C. The average hydrodynamic diameters of DOX@MSNs-COS-NN-CMC, DOX@MSNs-COS-SS-CMC and DOX@MSNs-COS-CMC-SS were about 220 ± 30 nm with narrow size distribution. In addition, the obtained nanoparticles exhibited core-shell structures in the TEM images, the particle sizes were around 100 ± 30 nm.

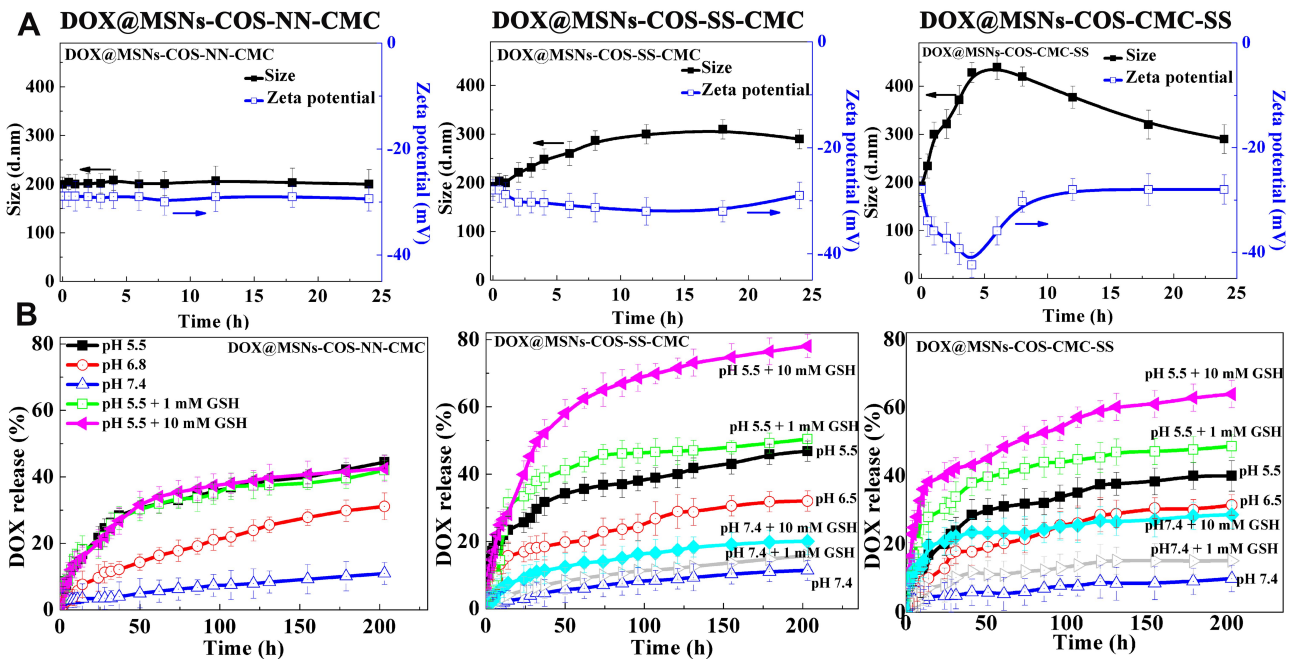

Figure 3 Drug release analysis of DOX@MSNs-COS-NN-CMC, DOX@MSNs-COS-SS-CMC and DOX@MSNs-COS-CMC-SS. (**A**) Particle size and zeta potential variation of DOX-loaded nanoparticles at pH 7.4 and 10 mM GSH. (**B**) Drug release of DOX-loaded nanoparticles at different pH and glutathione variation.

Abbreviations: MSNs, mesoporous silica nanoparticles; DOX, doxorubicin hydrochloride; COS, chitosan oligosaccharide; COS-SS, disulfide-containing chitosan oligosaccharide; COS-NN, non-cleavable chitosan, diallyl disulfide was replaced by N,N′-methylenebisacrylamide; CMC, carboxymethyl chitosan; CMC-SS, disulfide-containing carboxymethyl chitosan; GSH, glutathione.

Moreover, charge reversal was clearly observed in DOX@MSNs-COS-NN-CMC, DOX@MSNs-COS-SS-CMC and DOX@MSNs-COS-CMC-SS (Figure 2D). The zeta potential of DOX-loaded nanoparticles reversed from −24 mV to 10 mV when the pH value was changed from 7.4 to 6.5, which is related to the amino groups of DOX (pKa, 8.3) and COS (pKa, 6.5) and the carboxyl groups of CMC (pKa, 4.0; DS, 92%; Y_{-NH2}, 56%). In addition, the particle size was reduced with the decreasing pH value with a minimum of 150 nm at pH 5.5, after that the particle size was slightly increased, which is attributed to the electrostatic effect and the curl of the molecular chain. The charge reversal, particle shrinking-swelling and redox characteristics would prolong retention time, promote intracellular uptake and stimulate DOX delivery to nucleus.

Effects of Disulfide Bonds Location on in vitro Drug Release

As shown in Figure 3A, negligible zeta potential and size changes of DOX@MSNs-COS-NN-CMC were observed when an intracellular level of GSH presented in phosphate buffer solution (pH 7.4). However, DOX@MSNs-COS-CMC-SS were rapidly disassembled into loose polymer with a wide size distribution and the surface charges were constantly decreased at pH 7.4 and 10 mM GSH after 4 h incubation, suggesting the reduction cleavage of disulfide bonds of CMC-SS.

Moreover, in vitro DOX releases from DOX@MSN-COS-SS-CMC and DOX@MSN-COS-CMC-SS were significantly correlated with the presence or absence of GSH and the pH values of solution, indicating the redox/pH dual-responsive drug release characteristics (Figure 3B). Drug release rate of DOX@MSN-COS-SS-CMC significantly reached 45% at pH 5.5, which was 3.5-fold higher than that at pH 7.4 (10%). Moreover, the release rate (78%) at pH 5.5 and 10 mM GSH was almost 7-fold higher than that at pH 7.4 after 200 h. Nevertheless, the drug leakage of DOX@MSN-COS-CMC-SS was clearly observed under the reduction condition, the DOX release rate was dramatically increased to 20% at pH 7.4 and 10 mM GSH within 14 h. Reversely, the DOX release of DOX@MSN-COS-CMC-SS (63%) was relatively lower than that of DOX@MSN-COS-SS-CMC at pH 5.5 and 10 mM GSH after 200 h.

The kinetics models of drug release from DOX@MSNs-COS-SS-CMC and DOX@MSNs-COS-CMC-SS were analyzed by comparing the correlation coefficient (R^2) and diffusion exponents. As shown in Table S2, the drug release from above multi-responsive nanoparticles conformed to Ritger-Peppas model. The R^2 of DOX@MSNs-COS-SS-CMC at pH

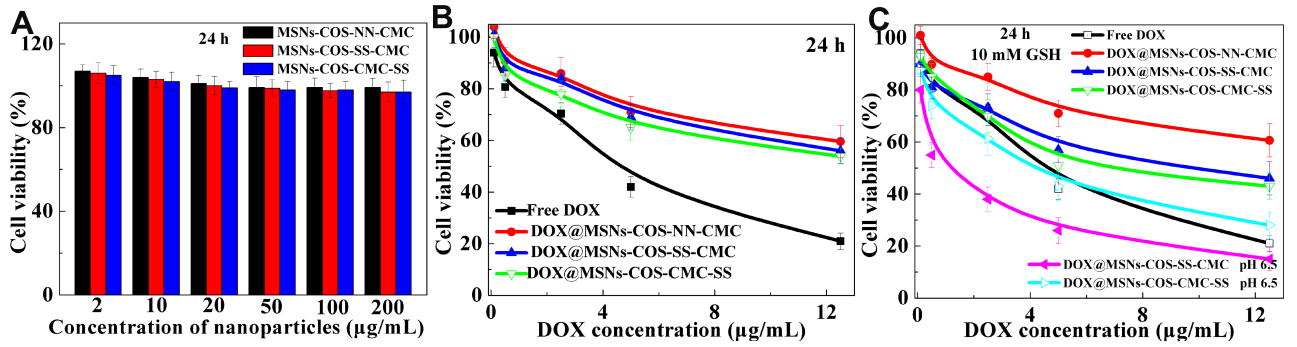

Figure 4 Cytotoxicity of blank and DOX-loaded nanoparticles in HeLa cells at 24 h. (**A**) In vitro viability of blank nanoparticles. (**B** and **C**) Cytotoxicity of DOX-loaded nanoparticles under different conditions.

Abbreviations: MSNs, mesoporous silica nanoparticles; DOX, doxorubicin hydrochloride; COS, chitosan oligosaccharide; COS-SS, disulfide-containing chitosan oligosaccharide; COS-NN, non-cleavable chitosan, diallyl disulfide was replaced by N,N′-methylenebisacrylamide; CMC, carboxymethyl chitosan; CMC-SS, disulfide-containing carboxymethyl chitosan; GSH, glutathione.

5.5 and 10 mM GSH was 0.61, revealing a non-Fick diffusion. The controllable drug delivery system of DOX@MSNs-COS-SS-CMC could be classified as a relatively complex matrix type under acidic and reduction conditions, which might involve swelling, diffusion and corrosion. However, the R^2 of DOX@MSNs-COS-SS-CMC at pH 7.4 and 10 mM GSH was 0.38, revealing a Fick release behavior. In addition, the drug release mechanism of DOX@MSNs-COS-CMC-SS at pH 7.4 and 5.5 containing 10 mM GSH fitted the Fick diffusion model. The difference in the release mechanism might be attributed to the disulfide bonds location of DOX@MSNs-COS-SS-CMC and DOX@MSNs-COS-CMC-SS.

The above results indicate that the disulfide bonds of DOX@MSN-COS-SS-CMC could be shielded by the CMC shell, which would prolong the circulation time and limit drug release in the extracellular microenvironment and promote the DOX accumulation at tumor sites.

Effects of Disulfide Bonds Location on Cytotoxicity and Intracellular Uptake

In view of the favorable biocompatibility of chitosan shell, the cell viability of blank MSNs-COS-NN-CMC, MSNs-COS-SS-CMC and MSNs-COS-CMC-SS were high around 90% (Figure 4A). Both free DOX and DOX-loaded nanoparticles exhibited a clear time and dosage-dependent cytotoxicity in HeLa cells (Figure 4B and C). In comparison with free DOX, DOX-loaded nanoparticles still exhibited lower toxicity, which was mainly attributed to the gradual drug release, thus inducing effective drug transportation during blood circulation. However, the cytotoxicity of DOX@MSNs-COS-SS-CMC was apparently increased at pH 6.5 and 10 mM GSH after 24 h incubation (Figure 4C).

The intracellular uptake of DOX-loaded nanoparticles in HeLa cells was evaluated by CLSM technique (Figure 5A and B). As shown in Figure 5A, red fluorescence was observed in the nuclei after incubated with free DOX at pH 7.4 for 24 h, which would interfere with the process of DNA replication and induce the cell apoptosis. In contrast, the DOX fluorescence of DOX@MSNs-COS-NN-CMC, DOX@MSNs-COS-SS-CMC and DOX@MSNs-COS-CMC-SS were primarily located in the cytoplasm and slightly accumulated in the perinuclear region. However, the DOX fluorescence in the cell nucleus gradually increased when DOX@MSNs-COS-SS-CMC and DOX@MSNs-COS-CMC-SS were incubated at pH 7.4 and 10 mM GSH (Figure 5B), due to the rapid cleavage of disulfide bonds in response to the intracellular reduction microenvironment. Furthermore, DOX was burst into release at pH 6.5 and 10 mM GSH, which was attributed to the pH-triggered charge-reversal of DOX@MSNs-COS-SS-CMC and DOX@MSNs-COS-CMC-SS, thus facilitating endosomal escape and promote DOX transformation into cellular nucleus via the enhanced penetration effect or the interaction with endosomal membrane during intracellular uptake.

A similar phenomenon was observed in the flow cytometry analysis (Figure 5C and D). Since free DOX has no selectivity, the mean fluorescence intensity (MFI) of DOX@MSNs-COS-SS-CMC and DOX@MSNs-COS-CMC-SS at pH 7.4 and 10 mM GSH were 0.7-fold and 0.8-fold higher than that of free DOX after 24 h, respectively. Moreover, the MFI of DOX@MSNs-COS-SS-CMC and DOX@MSNs-COS-CMC-SS at pH 6.5 and 10 mM GSH were 1.9-fold and 1.3-fold higher than that of free DOX, respectively.

The results indicate that MSNs-COS-SS-CMC may require a long period to locate in the nuclei of cancer cells at pH 7.4 due to the firm encapsulation. However,

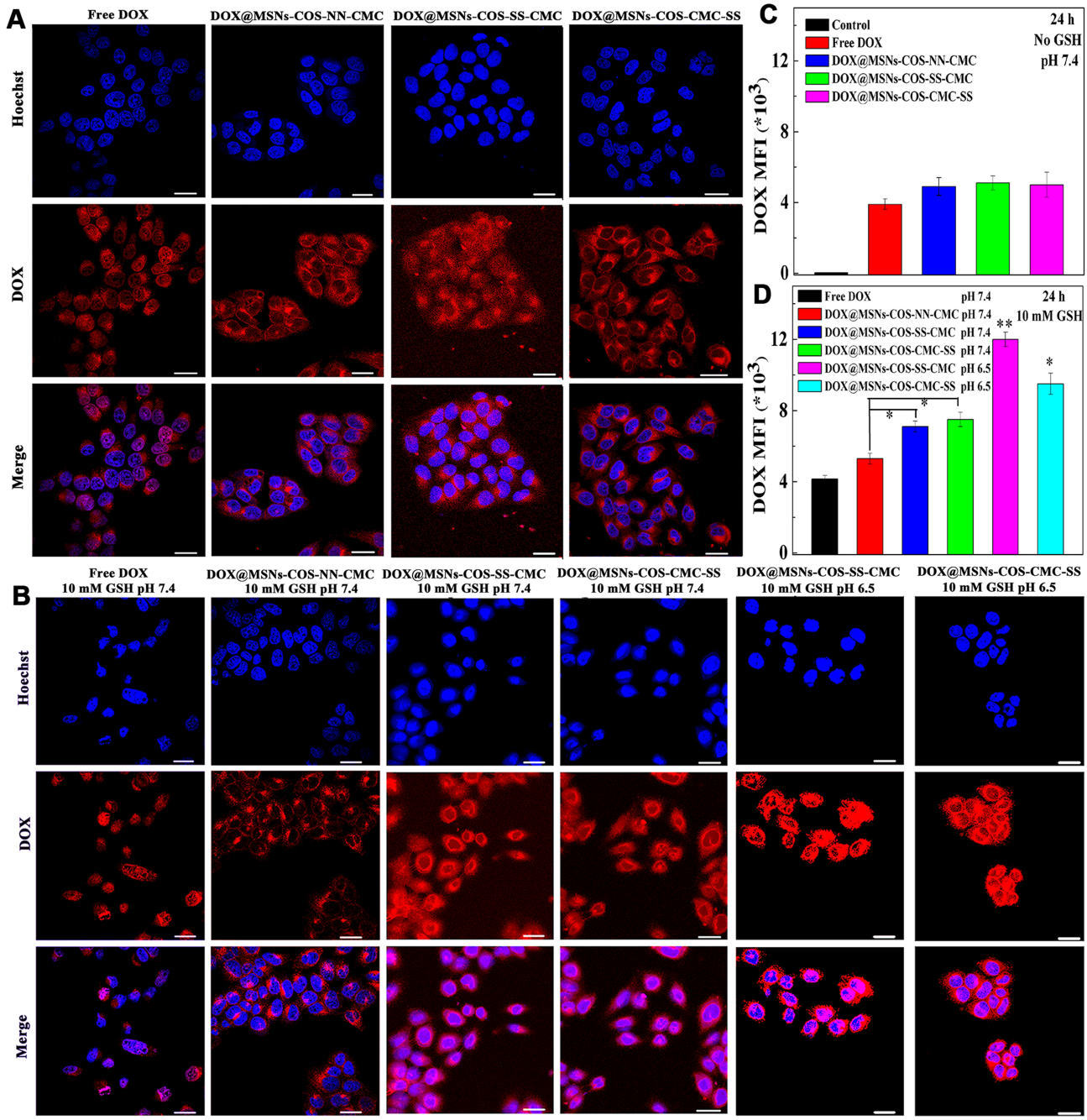

Figure 5 Intracellular distribution of DOX-loaded nanoparticles in HeLa cells. (**A** and **B**) CLSM images in HeLa cells (DOX, 2 μg/mL; Scale bar, 20 μm). (**C** and **D**) The mean fluorescence intensity (MFI) of DOX (DOX, 2 μg/mL). Data are presented as the mean value ± standard deviation (n=3). *Means P < 0.05 and **Means P <0.01, compared with the control group.

Abbreviations: MSNs, mesoporous silica nanoparticles; DOX, doxorubicin hydrochloride; COS, chitosan oligosaccharide; COS-SS, disulfide-containing chitosan oligosaccharide; COS-NN, non-cleavable chitosan, diallyl disulfide was replaced by N,N′-methylenebisacrylamide; CMC, carboxymethyl chitosan; CMC-SS, disulfide-containing carboxymethyl chitosan; GSH, glutathione.

MSNs-COS-SS-CMC could significantly trigger effective DOX release into nucleus at pH 6.5 and 10 mM GSH due to the cascade-targeting of pH-triggered charge-reversible and redox character. The design of cascade-targeting and the shielding of disulfide bonds would minimize side effects of chemotherapeutic drugs and provide a potential in human cervical carcinoma therapy without frequent drug administration.

Intracellular Tracking of DOX@MSNs-COS-SS-CMC

Nucleus and lysosome were labeled by Hoechst and LysoTracker Green, respectively, to investigate the endosomal escapes of DOX@MSNs-COS-NN-CMC, DOX@MSNs-COS-SS-CMC and DOX@MSNs-COS-CMC-SS. The pixel intensity profiles were obtained by the colocalization of image J software to evaluate the fluorescence intensity and localization. As illustrated in Figure 6 and S4, S5, the red DOX fluorescence was almost overlapped with Green LysoTracker fluorescence after the incubation of HeLa cells with DOX-loaded nanoparticles for 1 h, which demonstrated that nanoparticles were stranded in the endo/lysosomes. However, the DOX fluorescence of DOX-loaded nanoparticles was clearly separated from the LysoTracker fluorescence as the incubation time extended to 3 h, which indicated that the above nanoparticles could subsequently escape from lysosome to cytoplasm. In

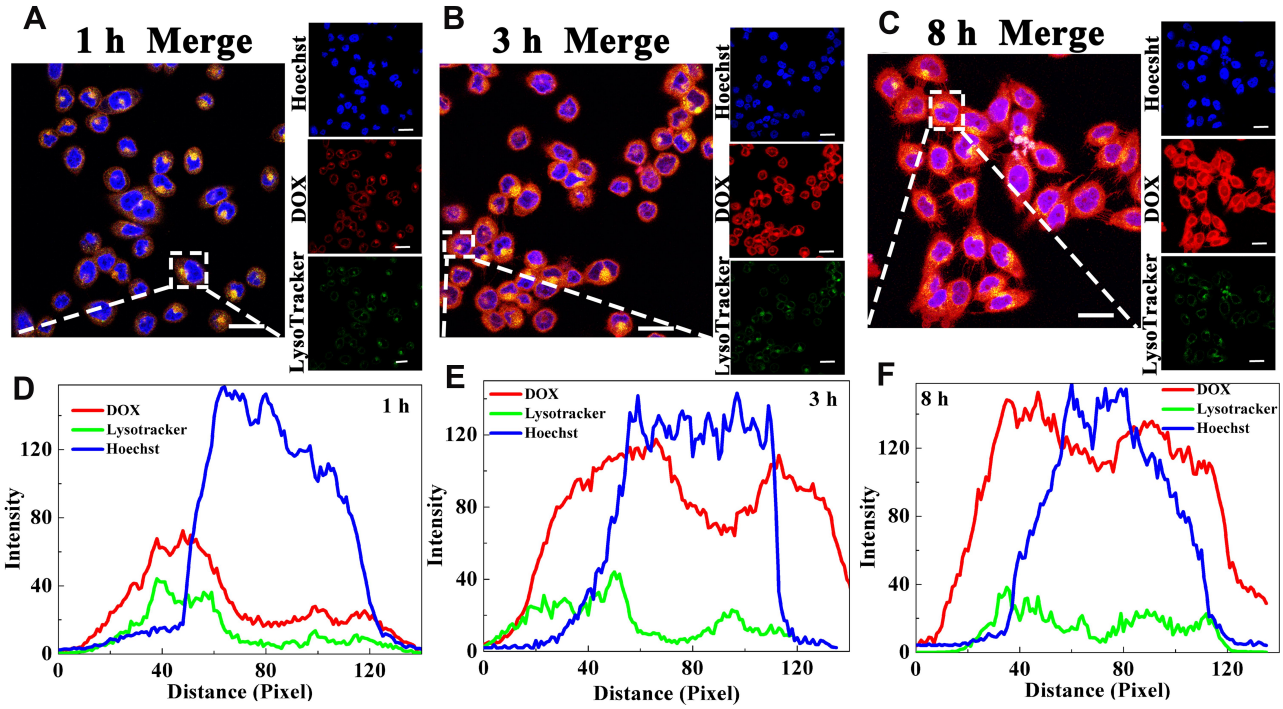

Figure 6 Endosomal escape of DOX@MSNs-COS-SS-CMC in HeLa cells at pH 6.5 and 10 mM GSH for different time courses. (**A**–**C**) Confocal microscopic images. (**D**–**F**) Pixel intensity profiles. (DOX, 2 μg/mL; Scale bar, 20 μm).

Abbreviations: MSNs, mesoporous silica nanoparticles; DOX, doxorubicin hydrochloride; COS-SS, disulfide-containing chitosan oligosaccharide; CMC, carboxymethyl chitosan; GSH, glutathione.

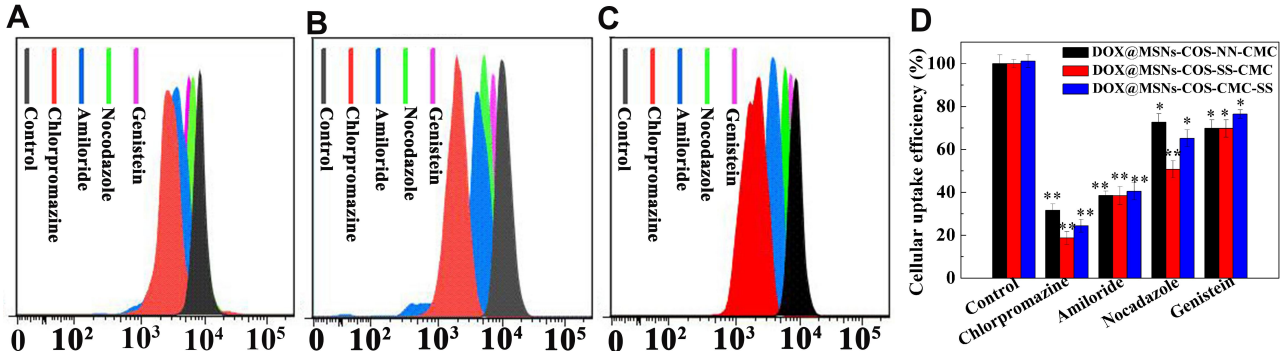

Figure 7 Endocytosis of DOX-loaded nanoparticles in HeLa cells at pH 6.5 and 10 mM GSH. The internalized DOX signals of (**A**) DOX@MSNs-COS-NN-CMC, (**B**) DOX@MSNs-COS-SS-CMC and (**C**) DOX@MSNs-COS-CMC-SS by flow cytometry. (**D**) Effect of endocytic inhibitors on cellular uptake efficiency. Data are presented as the mean value ± standard deviation (n=3). *Means $P < 0.05$ and **Means $P < 0.01$, compared with the control group.

Abbreviations: MSNs, mesoporous silica nanoparticles; DOX, doxorubicin hydrochloride; COS, chitosan oligosaccharide; COS-SS, disulfide-containing chitosan oligosaccharide; COS-NN, non-cleavable chitosan, diallyl disulfide was replaced by N,N′-methylenebisacrylamide; CMC, carboxymethyl chitosan; CMC-SS, disulfide-containing carboxymethyl chitosan; GSH, glutathione.

addition, in view of the cascade-targeting and shielding of disulfide bonds, DOX@MSNs-COS-SS-CMC possessed a significantly increased DOX fluorescence in the nucleus after incubation for 8 h. The above results indicate that DOX@MSNs-COS-NN-CMC, DOX@MSNs-COS-SS-CMC and DOX@MSNs-COS-CMC-SS possessed the endosome escape capacity through the proton sponge effects of amino groups.

Effects of Disulfide Bonds Location on Endocytosis

The internalization of DOX-loaded nanoparticles DOX @MSNs-COS-NN-CMC, DOX@MSNs-COS-SS-CMC and DOX@MSNs-COS-CMC-SS was analyzed by flow cytometry to quantitatively evaluate the cellular uptake efficiency. HeLa cells were pretreated with endocytic inhibitors (chlorpromazine, amiloride, nocodazole and genistein) to interfere with the clathrin-mediated endocytosis, macropinocytosis, vesicular transport and caveolin-mediated endocytosis, respectively.[35] As illustrated in Figure 7, the uptake efficiency of DOX@MSNs-COS-SS-CMC decreased to 18%, 38%, 50% and 69% after pretreated with the corresponding endocytic inhibitors, respectively. A similar phenomenon was observed in the endocytosis of DOX@MSNs-COS-NN-CMC and DOX@MSNs-COS-CMC-SS. However, after the endocytic inhibition, the uptake

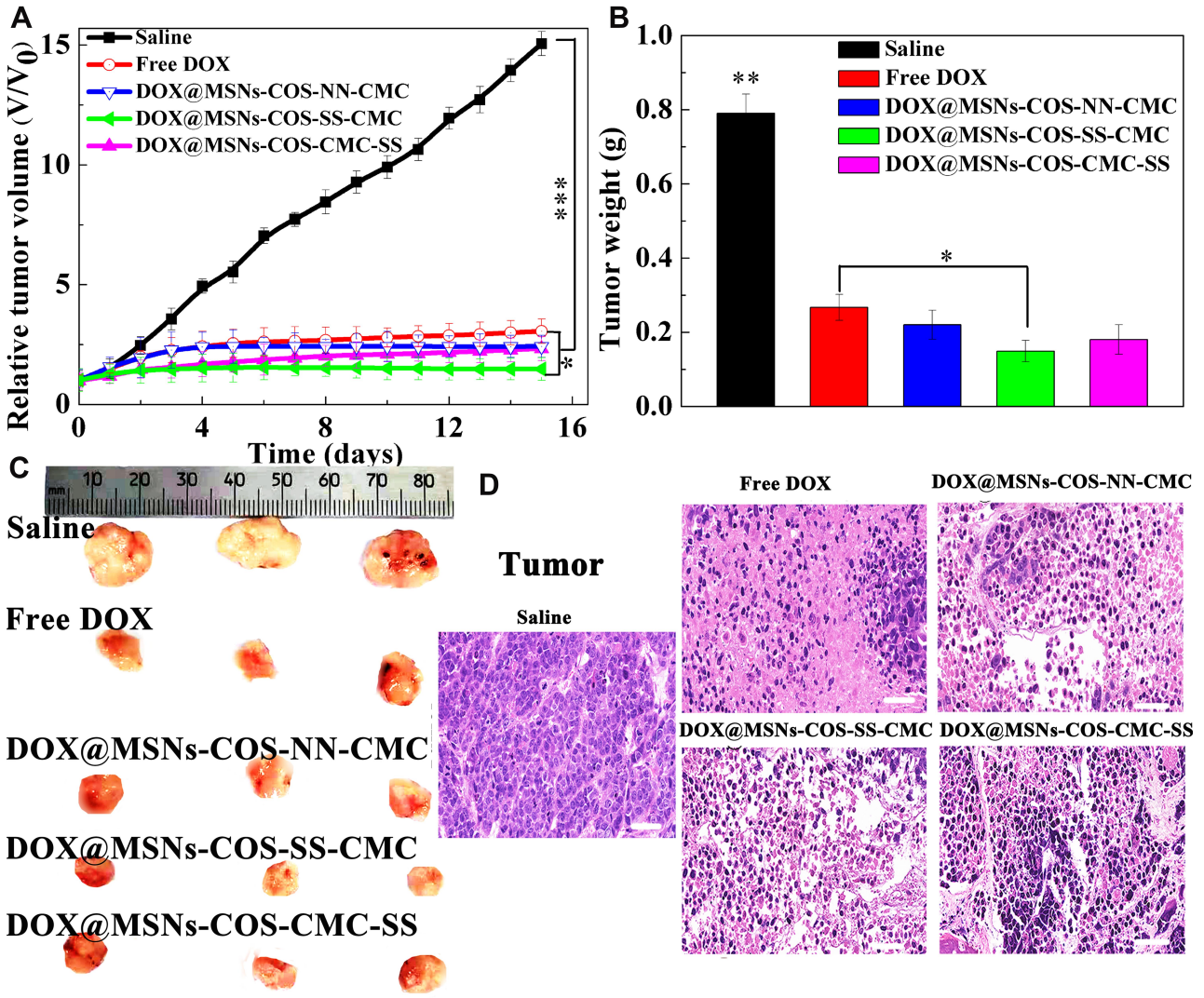

Figure 8 In vivo antitumor effects of DOX-loaded nanoparticles on HeLa tumor-bearing mice. (**A**) Relative tumor volumes after intravenous injection. Data are presented as the mean value ± standard deviation (n=3). *Means P < 0.05, **means P<0.01 and ***means P <0.001, compared with the control group. (**B**) Tumor weight. (**C**) Tumors images stripped from mice after 15 days. (**D**) H&E staining analysis of tumor (Scale bar, 50 μm).

Abbreviations: MSNs, mesoporous silica nanoparticles; DOX, doxorubicin hydrochloride; COS, chitosan oligosaccharide; COS-SS, disulfide-containing chitosan oligosaccharide; COS-NN, non-cleavable chitosan, diallyl disulfide was replaced by N,N′-methylenebisacrylamide; CMC, carboxymethyl chitosan; CMC-SS, disulfide-containing carboxymethyl chitosan.

efficiency of DOX@MSNs-COS-CMC-SS decreased to 24%, 40%, 65% and 76%, respectively. The results reveal that clathrin-mediated endocytosis and macropinocytosis are the main endocytosis pathway of the above DOX-loaded nanoparticles in HeLa cells. In addition, vesicular transport might be a factor that affects the difference in uptake efficiency of DOX@MSNs-COS-SS-CMC and DOX@MSNs-COS-CMC-SS.

Antitumor Evaluation in vivo

The tumor accumulation and biocompatibility of free DOX and DOX-loaded nanoparticles were investigated in HeLa tumor-bearing nude mice. As shown in Figure S6, the DOX fluorescence of free DOX was substantially accumulated in the normal tissues and tumor, but due to the short half-life of DOX in the blood circulation,[37] the DOX fluorescence was rapidly eliminated after 3 h. Whereas, the DOX fluorescence signals of DOX@MSNs-COS-SS-CMC reached to the maximum after 12 h post injection, which indicates a preeminent tumor targeting efficiency and long blood circulation. The DOX fluorescence in liver and spleen was relatively increased after 24 h, indicating that DOX@MSNs-COS-SS-CMC were gradually eliminated by reticuloendothelial system-rich organs.

As shown in Figure 8A, the tumor volume of the control group rapidly soared from 100 to 1500 mm^3 after 15 days, whereas the tumor volume of DOX@MSNs-COS-SS-CMC (140 mm^3) was relatively smaller than that of free DOX (290 mm^3). Moreover, tumor weight of DOX@MSNs-COS-SS-CMC (0.13 g, Figure 8B) was the lowest in these five groups (control, 0.79 g; free DOX, 0.28 g; DOX@MSNs-COS-NN-CMC, 0.22 g; DOX@MSNs-COS-CMC-SS, 0.19 g). In particular, the tumor size of DOX@MSNs-COS-SS-CMC was the smallest as directly visualized in the representative images (Figure 8C). In addition, H&E staining and histological examination of tumor tissues were conducted to further verify the antitumor mechanism of each group (Figure 8D). In comparison with the regular structure in the control group, different degrees of apoptosis or necrosis with cell

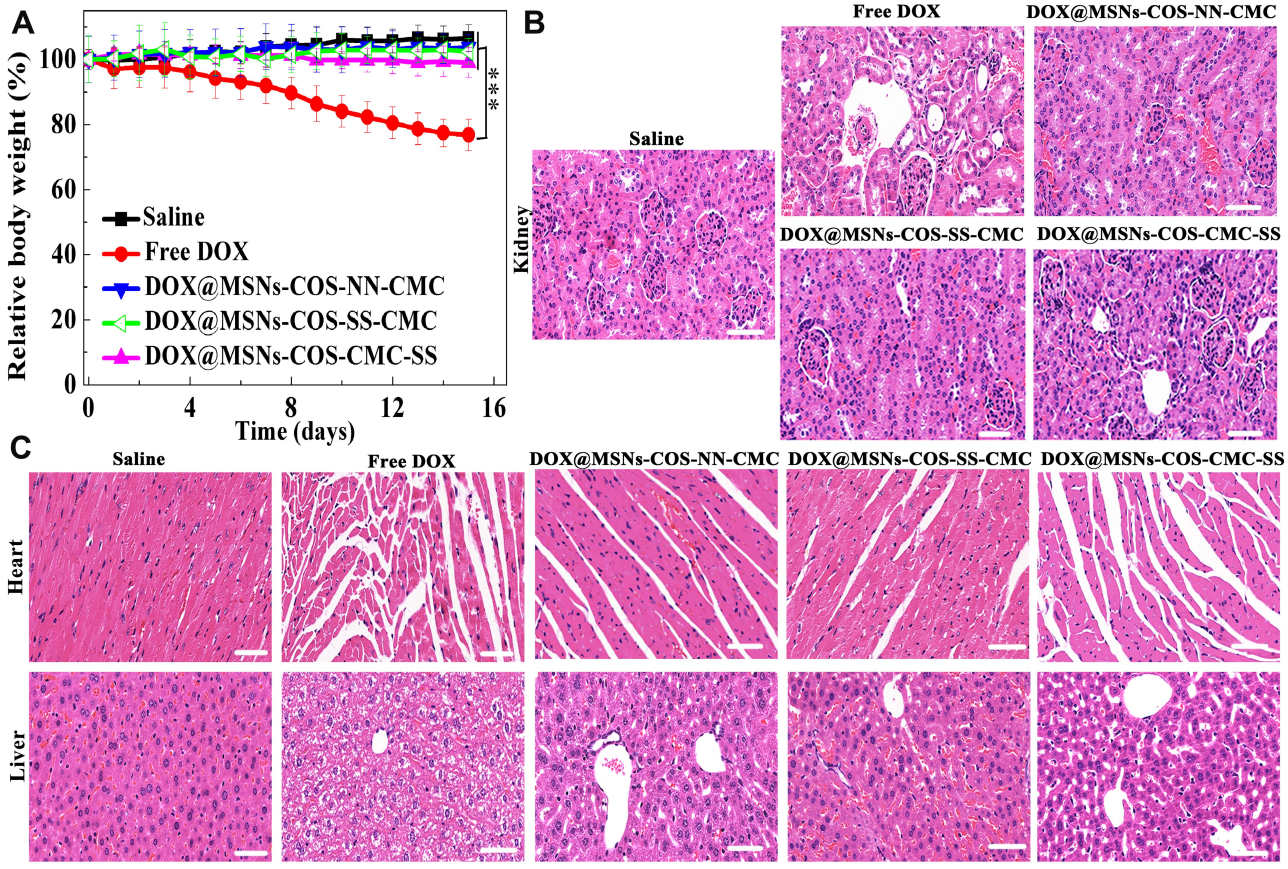

Figure 9 Biosafety analysis of DOX-loaded nanoparticles in HeLa tumor-bearing mice. (**A**) Changes of body weight. Data are presented as the mean value ±standard deviation (n=3). ***Means P <0.001, compared with the control group. (**B** and **C**) H&E staining analysis of kidney, heart and liver (Scale bar, 50 μm).

Abbreviations: MSNs, mesoporous silica nanoparticles; DOX, doxorubicin hydrochloride; COS, chitosan oligosaccharide; COS-SS, disulfide-containing chitosan oligosaccharide; COS-NN, non-cleavable chitosan, diallyl disulfide was replaced by N,N′-methylenebisacrylamide; CMC, carboxymethyl chitosan; CMC-SS, disulfide-containing carboxymethyl chitosan.

vacuolization and karyopyknosis were observed in DOX-treated groups. Whereas DOX@MSNs-COS-SS-CMC presented a maximum range of vacuolization and looser structure than other groups. The results show that DOX@MSNs-COS-SS-CMC possessed higher tumor suppression effect than free DOX, DOX@MSNs-COS-NN-CMC and DOX@MSNs-COS-CMC-SS.

Moreover, there was no significant weight loss in the DOX@MSNs-COS-SS-CMC group (Figure 9A), indicating a potential for clinical application without side effect. The biosafety was also evaluated by histological analysis of kidney, heart and liver (Figure 9B and C). Severe side effects were observed in the free DOX group: acute pyogenic lesion in kidney, myocardial fibers arranged irregularly and distributed unevenly; focal necrosis in liver. In addition, histopathological changes were also observed in the DOX@MSNs-COS-CMC-SS group due to the drug leakage in normal tissue. However, pathological changes and injuries were negligible in the DOX@MSNs-COS-SS-CMC group, indicating the synergistic targeting ability without cardiotoxicity.

The results confirm that charge reversible and pH/redox sensitive DOX@MSNs-COS-SS-CMC would provide a potential to improve the specificity, efficacy and safety in human cervical carcinoma therapy through the cascade-targeting and disulfide bonds shielding.

Conclusion

In summary, cancer-specific delivery system has been rationally designed for pinpointed cascading-controlled drug release through pH-triggered charge-reversal and redox-responsive DOX@MSNs-COS-SS-CMC. This simplified drug loading procedure was able to overcome significant biological barriers including the intracellular uptake and cytoplasmic degradation. Vesicular transport might be a factor that affects the difference in uptake efficiency of DOX@MSNs-COS-SS-CMC and DOX@MSNs-COS-CMC-SS. In vitro and in vivo study confirmed that the multi-responsive DOX@MSNs-COS-SS-CMC could not only improve the accumulation and retention time at tumor site in the HeLa bearing mice but also attenuate the DOX leakage in the heart and liver via the cleavage of disulfide linkage. Thus, this work possesses high potential in versatile drug delivery for alleviating the main dose-limiting cardiotoxicity without compromising the therapeutic efficacy in clinical therapy.

Funding

This research was supported by the National Natural Science Foundation of China (grant nos. 1504527, 51703207 and 21803060) and Zhongyuan Science and Technology Innovation Leading Talents Project (194200510030).

Disclosure

The authors report no conflicts of interest for this work.

References

1. Chen W-H, Yu X, Cecconello A, Sohn YS, Nechushtai R, Willner I. Stimuli-responsive nucleic acid-functionalized metal–organic framework nanoparticles using pH- and metal-ion-dependent DNAzymes as locks. *Chem Sci*. 2017;8(8):5769–5780. doi:10.1039/C7SC01765K
2. Lee S, Ahn RW, Chen F, et al. Biological evaluation of pH-responsive polymer-caged nanobins for breast cancer therapy. *ACS Nano*. 2010;4(9):4971–4978. doi:10.1021/nn100560p
3. Han L, Tang C, Yin C. Dual-targeting and pH/redox-responsive multi-layered nanocomplexes for smart co-delivery of doxorubicin and siRNA. *Biomaterials*. 2015;60:42–52. doi:10.1016/j.biomaterials.2015.05.001
4. Zhang W, Lu J, Gao X, Li P, Tang B. Enhanced photodynamic therapy by reduced intracellular glutathione levels employing nano-MOF with Cu (II) as active center. *Angew Chem Int Edit*. 2018;130(18):4985–4990. doi:10.1002/ange.201710800
5. Liu Y, Terrell JL, Tsao C-Y, et al. Biofabricating multifunctional soft matter with enzymes and stimuli-responsive materials. *Adv Func Mater*. 2012;22(14):3004–3012. doi:10.1002/adfm.201200095
6. Pramod PS, Shah R, Jayakannan M. Dual stimuli polysaccharide nanovesicles for conjugated and physically loaded doxorubicin delivery in breast cancer cells. *Nanoscale*. 2015;7(15):6636–6652. doi:10.1039/C5NR00799B
7. Deng YH, Yang WL, Wang CC, Fu SK. A novel approach for preparation of thermoresponsive polymer magnetic microspheres with core–shell structure. *Adv Mater*. 2003;15(20):1729–1732. doi:10.1002/adma.200305459
8. Nagase K, Yamato M, Kanazawa H, Okano T. Poly(N -isopropylacrylamide)-based thermoresponsive surfaces provide new types of biomedical applications. *Biomaterials*. 2018;153:27–48. doi:10.1016/j.biomaterials.2017.10.026
9. Xin J, Wang S, Wang B, Wang J, Yao C. AlPcS4-PDT for gastric cancer therapy using gold nanorod, cationic liposome, and Pluronic F127 nanomicellar drug carriers. *Int J Nanomed*. 2018;13:2017–2036. doi:10.2147/IJN.S154054
10. Kim KS, Kim J, Lee JY, et al. Stimuli-responsive magnetic nanoparticles for tumor-targeted bimodal imaging and photodynamic/hyperthermia combination therapy. *Nanoscale*. 2016;8(22):11625–11634. doi:10.1039/C6NR02273A
11. Feng Q, Zhang Y, Zhang W, Shan X, Yuan Y. Tumor-targeted and multi-stimuli responsive drug delivery system for near-infrared light induced chemo-phototherapy and photoacoustic tomography. *Acta Biomater*. 2016;38:129–142. doi:10.1016/j.actbio.2016.04.024
12. Un K, Kawakami S, Suzuki R, Maruyama K, Yamashita F, Hashida M. Development of an ultrasound-responsive and mannose-modified gene carrier for DNA vaccine therapy. *Biomaterials*. 2010;31(30):7813–7826. doi:10.1016/j.biomaterials.2010.06.058
13. Yin T, Wang P, Li J, et al. Tumor-penetrating codelivery of siRNA and paclitaxel with ultrasound-responsive nanobubbles hetero-assembled from polymeric micelles and liposomes. *Biomaterials*. 2014;35(22):5932–5943. doi:10.1016/j.biomaterials.2014.03.072

14. Birts CN, Nijjar SK, Mardle CA, et al. A cyclic peptide inhibitor of C-terminal binding protein dimerization links metabolism with mitotic fidelity in breast cancer cells. *Chemi Sci*. 2013;4(8):3046–3057. doi:10.1039/c3sc50481f
15. Fang Z, Li X, Xu Z, et al. Hyaluronic acid-modified mesoporous silica-coated superparamagnetic Fe3O4 nanoparticles for targeted drug delivery. *Int J Nanomed*. 2019;14:5785–5797. doi:10.2147/IJN.S213974
16. Guan Y, Su Y, Zhao L, Meng F, Luo J. Biodegradable polyurethane micelles with pH and reduction responsive properties for intracellular drug delivery. *Mat Sci Eng C Mater*. 2017;75:1221–1230. doi:10.1016/j.msec.2017.02.124
17. Chan N, Khorsand B, Aleksanian S, Oh JK. A dual location stimuli-responsive degradation strategy of block copolymer nanocarriers for accelerated release. *Chem Commun*. 2013;49(68):7534–7536. doi:10.1039/c3cc44200d
18. Zhou W, Cui H, Ying L, Yu X. Enhanced cytosolic delivery and release of CRISPR/Cas9 by black phosphorus nanosheets for genome editing. *Angew Chem Int Ed*. 2018;57(32):10268–10272. doi:10.1002/anie.201806941
19. Liu Y, Xu C-F, Iqbal S, Yang X-Z, Wang J. Responsive nanocarriers as an emerging platform for cascaded delivery of nucleic acids to cancer. *Adv Drug Deliver Rev*. 2017;115(115):98–114. doi:10.1016/j.addr.2017.03.004
20. Zhao X, Wei Z, Zhao Z, et al. Design and development of graphene oxide nanoparticle/chitosan hybrids showing pH-sensitive surface charge-reversible ability for efficient intracellular doxorubicin delivery. *ACS Appl Mater Inter*. 2018;10(7):6608–6617. doi:10.1021/acsami.7b16910
21. Feng W, Zhou X, He C, et al. Polyelectrolyte multilayer functionalized mesoporous silica nanoparticles for pH-responsive drug delivery: layer thickness-dependent release profiles and biocompatibility. *J. Mater Chem B*. 2013;1(43):5886–5898. doi:10.1039/c3tb21193b
22. Xu C, Song R, Lu P, et al. pH-triggered charge-reversal and redox-sensitive drug release polymer micelles co-deliver doxorubicin and triptolide for prostate tumor therapy. *Int J Nanomed*. 2018;13:7229–7249. doi:10.2147/IJN.S182197
23. Ma B, Zhuang W, Wang Y, Luo R, Wang Y. pH-sensitive doxorubicin-conjugated prodrug micelles with charge-conversion for cancer therapy. *Acta Biomater*. 2018;70:186–196. doi:10.1016/j.actbio.2018.02.008
24. Fang L, Chen W, You B, Yang L, Zhang X-N. Enhanced cellular internalization and on-demand intracellular release of doxorubicin by stepwise pH-/reduction-responsive nanoparticles. *ACS Appl Mater Inter*. 1944;8(47):32146–32158.
25. Li L, Raghupathi K, Yuan C, Thayumanavan S. Surface charge generation in nanogels for activated cellular uptake at tumor-relevant pH. *Chem Sci*. 2013;4(9):3654–3660. doi:10.1039/c3sc50899d
26. Tang Y, Hu H, Zhang MG, et al. An aptamer-targeting photoresponsive drug delivery system using "off–on" graphene oxide wrapped mesoporous silica nanoparticles. *Nanoscale*. 2015;7(14):6304–6310. doi:10.1039/C4NR07493A
27. Yang C, Gao S, Dagnæs-Hansen F, Jakobsen M, Kjems J. Impact of PEG chain length on the physical properties and bioactivity of PEGylated Chitosan/siRNA nanoparticles in vitro and in vivo. *ACS Appl Mater Inter*. 2017;9(14):12203–12216. doi:10.1021/acsami.6b16556
28. Jia M, Li Y, Yang X, et al. Development of both methotrexate and mitomycin C loaded PEGylated Chitosan nanoparticles for targeted drug codelivery and synergistic anticancer effect. *ACS Appl Mater Inter*. 2014;6(14):11413–11423. doi:10.1021/am501932s
29. Zhang M, Liu J, Kuang Y, et al. "Stealthy" chitosan/mesoporous silica nanoparticle based complex system for tumor-triggered intracellular drug release. *J Mater Chem B*. 2016;4(19):3387–3397. doi:10.1039/C5TB02548F
30. Wang F, Sun W, Li L, et al. Charge-reversible multi-functional HPMA copolymers for mitochondrial targeting. *ACS Appl Mater Inter*. 2017;9(33):27563–27574. doi:10.1021/acsami.7b09693
31. Sun L, Wang D, Chen Y, et al. Core-shell hierarchical mesostructured silica nanoparticles for gene/chemo-synergetic stepwise therapy of multidrug-resistant cancer. *Biomaterials*. 2017;133:219–228. doi:10.1016/j.biomaterials.2017.04.028
32. Cui L, Liu W, Liu H, et al. pH-triggered charge-reversal mesoporous silica nanoparticles stabilized by chitosan oligosaccharide/carboxymethyl chitosan hybrids for effective intracellular delivery of doxorubicin. *ACS Appl Bio Mater*. 2019;2(5):1907–1919. doi:10.1021/acsabm.8b00830
33. Wang H, Dai T, Li S, et al. Scalable and cleavable polysaccharide nanocarriers for the delivery of chemotherapy drugs. *Acta Biomater*. 2018;72:206–216. doi:10.1016/j.actbio.2018.03.024
34. Chen X-G, Park H-J. Chemical characteristics of O-carboxymethyl chitosans related to the preparation conditions. *Carbohyd Polym*. 2003;53(4):355–359. doi:10.1016/S0144-8617(03)00051-1
35. Tian Y, Wu M, Liu X, et al. Viral nanoparticles: probing the endocytic pathways of the filamentous bacteriophage in live cells using ratiometric pH fluorescent indicator. *Adv Healthc Mater*. 2015;4(3):413–419. doi:10.1002/adhm.201400508
36. Wang J, Wang X, Zhao G, et al. Polyvinylpyrrolidone and polyacrylamide intercalated molybdenum disulfide as adsorbents for enhanced removal of chromium(VI) from aqueous solutions. *Chem Eng J*. 2018;334:569–578. doi:10.1016/j.cej.2017.10.068
37. Yang D, Wang T, Su Z, Xue L, Mo R, Zhang C. Reversing cancer multidrug resistance in xenograft models via orchestrating multiple actions of functional mesoporous silica nanoparticles. *ACS Appl Mater Inter*. 2016;8(34):22431–22441. doi:10.1021/acsami.6b04885